Multiphase Flow Simulations Using the Meshfree Smoothed Particle Hydrodynamics Method

C. Hoefler*, S. Braun, R. Koch, H.-J. Bauer
Institute of Thermal Turbomachinery, Karlsruhe Institute of Technology, Germany
corina.hoefler@kit.edu

Abstract

In order to numerically simulate primary atomization a fully three-dimensional code based on the meshless, Lagrangian Smoothed Particle Hydrodynamics method [1] [2] has been developed and validated for various test cases. One of the main advantages of this approach compared to meshbased simulation methods is the inherent interface advection without the need for interface markers or interface capturing techniques. The present paper focuses on the capability of our code to accurately capture multiphase flow phenomena. For validation of the method regarding shear-driven flows the unsteady evolution of a Couette flow has been simulated successfully. Furthermore, surface tension effects in a multiphase system with a large density ratio of the gas-liquid mixture are modeled accurately. Moreover, the simulation of the disintegration process of a liquid film, driven by the surrounding air flow, at an atomizer edge has been performed. The results demonstrate the promising potential of the method to numerically predict the entire primary atomization in complex airblast atomizers.

Introduction

In the near future a massive increase in air traffic is expected. At the same time resources of fossil fuel will diminish and emission restrictions will become more stringent. These challenges lead to the need of new, innovative jet engine concepts. An optimized atomization of the liquid fuel is crucial to boost the engine efficiency. The primary atomization of the liquid film into ligaments and large droplets has a major effect on the spray quality and the resulting droplet size and velocity distributions. However, primary atomization itself cannot be measured explicitly. In order to design appropriate airblast atomizers, reliable numerical tools for the prediction of primary atomization are essential.

Numerical modeling of the primary atomization process is still not efficiently feasible for practical applications using gridbased methods. The interface capturing techniques, such as Volume of Fluid (VoF) or Level Set method, exhibit severe drawbacks. They suffer from complex and often inaccurate reconstruction of three-dimensional interfaces and mass loss, respectively. Inaccurate reconstruction of the interface causes deficiencies of the predicted interface curvature, which in turn results into erroneous representation of surface tension forces and thus inaccurate modeling of the primary atomization process. To minimize those errors and accurately capture the phenomena occurring during primary atomization the combination of these methods [3], adaptive grid refinement [4] and huge amounts of grid cells are necessary.

The meshfree, Lagrangian Smoothed Particle Hydrodynamics (SPH) approach is a promising alternative to overcome these shortcomings of gridbased methods. Different phases can be modeled easily by assigning an appropriate marker function and the according fluid properties to the corresponding discretization points. A huge benefit is the inherent advection of phase interfaces, as the discretization points or so called particles move with the velocity field of the fluid flow. Thus, there is no need for any interface tracking or capturing techniques. The SPH method has already been successfully validated for a shear-driven single phase flow inside a cavity and a qualitative comparison between the modeling of free surface flows and experiments has been conducted [5]. Within the present paper we focus on the capability of the method concerning multiphase flow simulations with particular emphasis on surface tension. The long-term objective is the development of a so called virtual atomizer test rig in order to avoid the cumbersome iterative process of nozzle design and repeated manufacturing.

Methodology

The Smoothed Particle Hydrodynamics method is a purely meshfree method, which has been developed in the field of astrophysics in the late 1970's. Computations are performed without the need of an underlying grid. The approach is based on the Lagrangian description of the governing equations. The fluid is discretized by an arbitrarily scattered set of spatially movable discretization points. Those so called particles represent a small

*Corresponding author: corina.hoefler@kit.edu

volume of the entire fluid domain. The physical properties of the fluid are assigned to those particles. The flow quantities at a certain location are interpolated from the neighboring discretization points via a weighting function. In the following the derivation of the basic SPH formulations, necessary for the transformation of the relevant governing equations, will be explained.

Mathematical approach

The flow properties are assumed to be described by an arbitrary function in space. Every spatial function $f(r)$ can be exactly reproduced by a convolution of the function itself with the Dirac function $\delta(r)$.

$$f(r) = \int f(r')\ \delta(r - r')dr' \tag{1}$$

In order to determine the physical quantities at position r, the neighboring discretization points at position r' have to be taken into account for the interpolation. Thus, the Dirac function is approximated by a so called kernel function $W(r - r', h)$, which weights the influence of the neighboring particle on the center particle. This yields the following integral approximation of a function:

$$f_i(r) = \int f(r')\ W(r - r', h)dr' \tag{2}$$

The kernel function has to fulfill some basic requirements [6] to ensure consistency and accuracy of the method. The smoothing length h defines the maximum radius of influence and thus the number of neighboring particles covered by the interpolation procedure.

In Fig. 1 an arbitrarily scattered set of discretization points is illustrated. The kernel function W is plotted for the center particle.

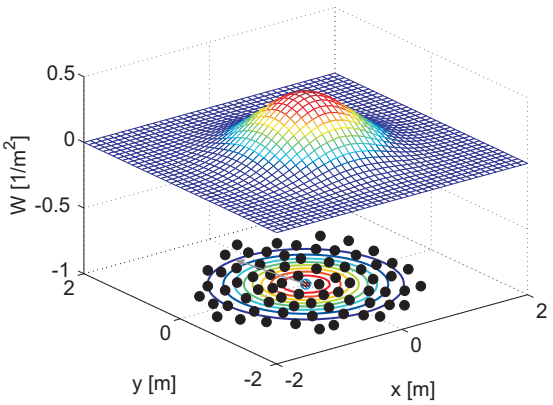

Figure 1. Kernel funtion for interpolation on center particle (blue)

In the final step the integral interpolant from Eq. 2 is transformed into a summation interpolant for numerical reasons. The summation is taken over all neighboring discretization points marked with the index b.

$$f_s(r) = \sum_b \frac{m_b}{\rho_b} f(r_b)\ W(r - r_b, h) \tag{3}$$

The same procedure applies for the SPH formulation of the gradient of a function.

$$\nabla f_s(r) = \sum_b \frac{m_b}{\rho_b} f(r_b)\ \nabla W(r - r_b, h) \tag{4}$$

Strictly speaking this is only valid, if the influence domain of a particle is not truncated by the discretized computational domain [6].

Formulation of governing equations

As the continuum assumption is valid, the Navier-Stokes equations can be used to describe the flow behavior. The continuity equation, the Navier-Stokes equations and the energy conservation equation are rewritten in a Lagrangian frame of reference for further treatment.

$$\frac{D\rho}{Dt} = -\rho\nabla\vec{v} \tag{5}$$

$$\frac{D\vec{v}}{Dt} = -\frac{\nabla p}{\rho} + \frac{\nabla\tau}{\rho} + \vec{f}_{ex} \tag{6}$$

$$\frac{Du}{Dt} = -\frac{p}{\rho}\,\nabla\vec{v} + \frac{\nabla\,(k\,\nabla T)}{\rho} + \frac{\Phi}{\rho} \tag{7}$$

The system of equations required for the complete description of the flow field will be closed using an appropriate equation of state to couple pressure and density explicitly.

Based on the formerly introduced basic SPH equations (Eqs. 3 and 4) and further mathematical transformations a variety of SPH compliant formulations of the conservation equations can be found in literature [7]. The important summation approximations for the density calculation and the pressure gradient term in the momentum equation are described briefly in the following. The approximated function will be set in <> brackets. The properties of the center particle itself are denoted with the index a, whereas the neighboring particles are marked with the index b. For clarity, the kernel function $W(r_a - r_b, h)$ and its gradient $\nabla W(r_a - r_b, h)$ are written in short as W_{ab} and ∇W_{ab}, respectively.

The density can either be calculated directly from a weighted summation over the neighboring particle masses or in accordance with the continuity equation Eq. 5. The first approach

$$\langle\rho\rangle_a = \sum_b m_b\, W_{ab} \tag{8}$$

conserves mass exactly. However, it is not suitable for free surface or multiphase calculations. Due to the particle deficiency at free surfaces or different masses assigned to particles of different phases, a non-physical density gradient normal to the interface will arise. This formulation can only be applied to single phase calculations in confined domains. The alternative continuity density approach results from the summation approximation of the RHS of Eq. 5.

$$\left\langle \frac{D\rho}{Dt} \right\rangle_a = \rho_a \sum_b \frac{m_b}{\rho_b}(\vec{v}_a - \vec{v}_b)\,\nabla W_{ab} \tag{9}$$

The formulation given here [8] has been applied to the multiphase test cases to be presented in the next section. Although it does not strictly conserve mass, which is negligible [9], it maintains the density discontinuities at free surfaces and phase interfaces. Similarly the formulation of the pressure gradient for multiphase flows can be derived. This yields

$$\left\langle \frac{D\vec{v}}{Dt} \right\rangle_a = \left\langle -\frac{\nabla p}{\rho} \right\rangle_a = -\sum_b m_b \frac{p_a + p_b}{\rho_a \rho_b}\,\nabla W_{ab} \tag{10}$$

in consistency with Eq. 9. Analogously, the summation approximations for all other terms in the momentum (Eq. 6) and energy equation (Eq. 7) are deduced.

The SPH method is based on a compressible approach. Pressure and density are coupled directly via an appropriate equation of state. In order to account for the incompressibility of liquids, they are modeled as weakly compressible. This is achieved via limitations of the numerical speed of sound c. The assumption of incompressibility is justified for maximum density variations below 1%. An estimation for c can be derived from the following relation.

$$M^2 = \frac{v^2}{c^2} \propto \frac{\Delta\rho}{\rho} \leq 1\% \tag{11}$$

Thus, the numerical speed of sound should be set to approximately $c \geq 10\ v_{max}$. On the other hand, the numerical speed of sound is usually lower than the physical speed of sound to avoid prohibitively small time steps due to the Courant-Friedrichs-Lewy condition.

The equation of state used for single phase computations without free surfaces is taken from [10].

$$p = c^2\rho \tag{12}$$

In case of free surfaces, the non-discretized space would act as a vacuum. A pressure gradient and thus acceleration of the particles normal to the surface would arise. For multiphase flows the pressure boundary condition at the phase interface $p_{phase0} = p_{phase1}$ might be violated.

Another pressure-density relation, originally derived for incompressible media [11], is given by the Tait equation of state.

$$\Delta p = \frac{c^2 \rho_0}{\gamma} \left[\left(\frac{\rho}{\rho_0} \right)^{\gamma} - 1 \right] \tag{13}$$

The advantage in comparison with Eq. 12 is its applicability to free surface and multiphase flow calculations, as it yields a relative pressure. Large oscillations in density cause strong pressure fluctuations. This results in large pressure gradients and thus large pressure driven forces among interacting particles. In response, the restoring force is larger, which restricts the density variations. This approach has been chosen for the multiphase test cases presented in the following section.

Surface tension

Surface tension forces play a dominant role for the numerical prediction of primary atomization. The interaction between aerodynamic and shear forces and the counteracting surface tension forces causes ligament breakup and droplet formation. For multiphase flow modeling we adopted the Continuum Surface Force (CSF) model of Brackbill et al. [12], which was originally proposed in the context of the VoF method. It is adapted for the SPH formulation in the form given in [13]. The additional force acting at the interface due to surface tension effects is

$$\left\langle \frac{D\vec{v}}{Dt} \right\rangle_{a,sf} = -\frac{\sigma}{\rho_a} \left(\nabla \cdot \hat{\vec{n}} \right)_a \vec{n}_a \tag{14}$$

A so called integer color index ζ is assigned to each particle according to the phase it belongs to. Subsequently, the normal vectors of the interface are derived from the smoothed color (ζ_s) field.

$$\langle \vec{n} \rangle_a = \sum_b \frac{m_b}{\rho_b} \frac{\zeta_{s,b} - \zeta_{s,a}}{|\zeta_b - \zeta_a|} \nabla W_{ab} \tag{15}$$

Applying further restrictions for error minimization [13], the divergence field of the normalized normal vectors $\nabla \cdot \hat{\vec{n}}$ is yielded. Thereafter, the additional force at the interface can be calculated according to Eq. 14.

Boundary conditions

In order to be able to model technically relevant fluid systems, appropriate boundary conditions (BC) have to be implemented. In the context of this paper the inlet / outlet boundary conditions will be explained in more detail. Whereas SPH is commonly dedicated to unbounded and confined domain fluid systems, the number of successfully conducted applications with inflow or outflow is still limited. In contrast to Eulerian methods, the physical properties of permeable boundaries cannot simply be set by assigning those properties to a surface. The Lagrangian nature of the method implies that particles have to be inserted into the domain or removed from the domain at a rate corresponding to the physical inflow and outflow. Our implementation follows the approach of Lastiwka et al. [14] and Hosseini and Feng [15]. The domain is extended upstream the inlet and downstream the outlet to avoid kernel truncation errors in the vicinity of these boundaries. The length of those so called buffer zones corresponds to the radius of influence. The desired physical BCs are imposed on the particles inside the buffer zones.

Inlet

First of all the inlet section has to be defined. For this purpose boundary markers are introduced, which in contrast to particles do not take part in the summation interpolations. They mark the boundary surface. Thus, arbitrarily located and shaped inlet boundaries are possible. Furthermore, each marker controls a certain number of particles located upstream of its position and ensures that the buffer zone is filled with particles. A Dirichlet boundary condition for a physical property is simply realized by assigning a value to the marker. All buffer particles receive the value of the marker they belong to. In our case a Dirichlet boundary condition is implemented for the fluid velocity and temperature. The value of the inflow property may change over time. To realize a Neumann boundary condition the value of the physical property at the boundary has to be known. This value is assigned upstream onto the preceding particles. To obtain the the physical property at a marker position, Eq. 3 is applied for

all neighboring particles inside the domain. Interpolation errors due to the truncation of the kernel are minimized by the use of a Shepard filter [16]. In the calculations to be presented in the next section the Neumann boundary condition is applied for the fluid density and pressure.

Outlet

Similar to the inlet, the outlet section is defined by boundary markers. Thus, the outlet may be arbitrarily shaped and located. The physical properties of the fluid at the outlet section are accessible via Eq. 3. In the examples to be discussed subsequently a Dirichlet BC is applied to the pressure. For the velocity a Neumann BC is required. It can be realized either by mapping the velocity at the markers onto the buffer particles downstream or, for a fully developed flow, by keeping velocity unchanged while crossing the buffer zone. Particles downstream the outlet buffer zone are removed.

Results and Discussion

Various test cases have been calculated with this SPH formulation. Each of them focuses on a distinctive fluid dynamic effect, which is crucial for the numerical modeling of primary atomization. The validated test cases prove the reliability and accuracy of the methodology. Moreover, the simulation of a technically relevant configuration demonstrates the promising potential of the method. The test cases will be discussed in order of increasing complexity.

Transient Couette flow

The temporal evolution of a planar Couette flow has been simulated, in order to validate the time-dependent behavior of shear-driven incompressible flows. The set up for those simulations, as depicted in Fig. 2, consists of a two-dimensional, square patch of liquid, which is confined by rigid walls on top and bottom and periodic boundaries (dash-dotted lines) at the left and right hand side of the domain. H represents the planar channel height. The bottom wall is static. The top wall is moving with the velocity u_0 in lateral direction.

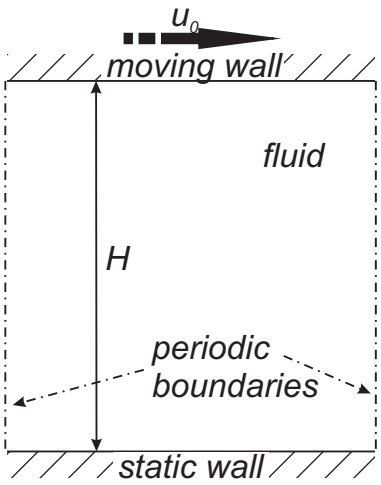

Figure 2. Numerical setup for Couette flow simulations

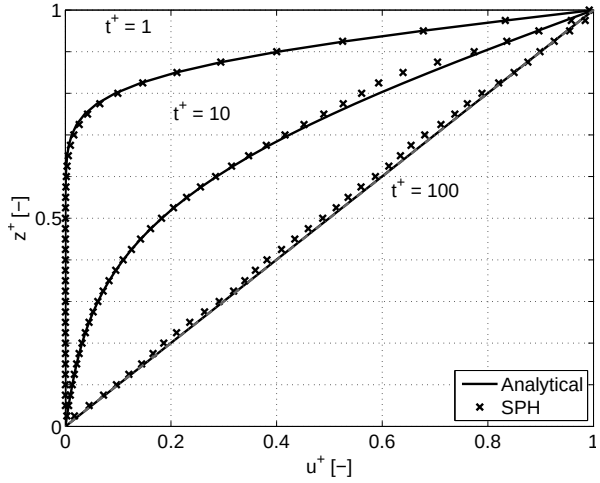

Figure 3. Transient velocity profiles of Couette flow for Re = 100

The fluid domain is discretized by 40 x 40 fluid particles to which the physical properties of water at standard ambient conditions are assigned. The interpolations are carried out with the quintic spline kernel [10] and a smoothing length of $h = 0.96 \cdot \Delta x$, where Δx represents the interparticle distance. The density is evaluated by the summation density approach given in Eq. 8 and coupled to the pressure field via Eq. 12. The Reynolds number has been varied by adjusting the velocity of the top wall, whereas density, domain dimensions and viscosity are kept constant. For validation of the transient SPH predictions, the SPH data (**x**) is mapped onto a cartesian grid and compared to time-dependent analytical solutions ($-$). The horizontal velocity profiles along a vertical sample line are illustrated in Fig. 3 for three timesteps $t^+ = t/0.007s$. The non-dimensional channel height is defined as $z^+ = z/H$ and the horizontal velocity u is normalized with the initial top wall velocity u_0, which yields $u^+ = u/u_0$. The results in the low Reynolds number regime are in excellent agreement with the analytical solutions. Minor deviations occur only in the transition region, between the lower discretization points at rest and

the already moving particles, for $t^+ = 1$. Proceeding in time those deviations become negligible. The no-slip boundary conditions at the walls are matched very well. Even for large velocity gradients, occurring close to the upper moving wall at the beginning of the simulation, the SPH method predicts the correct horizontal velocity profiles. For higher Reynolds numbers minor deviations are detected for steady state condition. This is due to the disordered particle distribution, which deteriorates the accuracy of the summation approximations and causes noise in the flow field. However, the results are still within 5%-tolerance of the analytical solution.

Droplet formation

To validate the SPH method in terms of multiphase systems and regarding the influence of surface tension, the following test case has been set up. Initially, a square patch of fluid 1 (red) is surrounded by fluid 0 (blue) (s. Fig. 4).

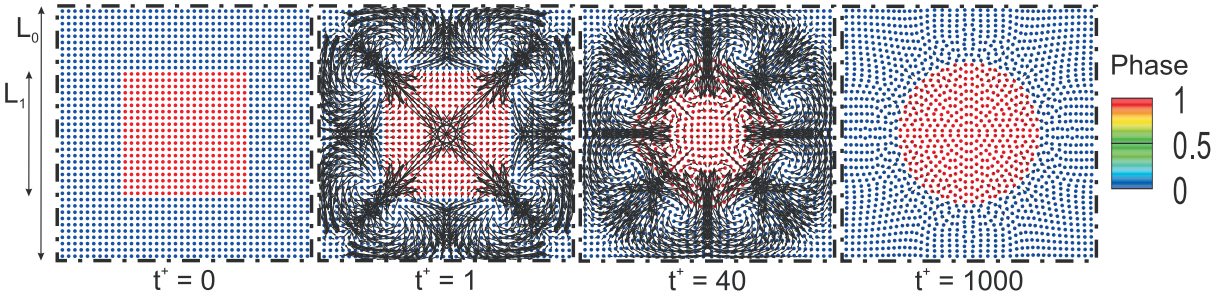

Figure 4. Particle distribution and velocity vectors for different time steps

The two-dimensional square computation domain exhibits periodic boundary conditions (dash-dotted lines) in both spatial directions. Domain dimensions are defined as $L_0 = 1 \cdot 10^{-2} m$ with $L_0/L_1 = 2$. Two phenomena, which are typical features of the presence of surface tension, are investigated. First of all the deformation of the initially square patch of fluid 1 into a disc should occur, due to the minimization of curvature and thus surface energy in the system. Secondly, the pressure jump across the curved interface, according to the Young-Laplace law, should be captured correctly. The density ratio of both phases is $\rho_1/\rho_0 = 1000$, corresponding to a fuel-air-mixture. Surface tension effects are taken into account via the Continuum Surface Force model [12] with the surface tension coefficient set to $\sigma = 0.07\ N/m$. As can be seen from the velocity vectors in the time series plot in Fig. 4 the surface tension forces impose large velocities, especially in regions of high curvature. This leads to spurious currents at the interface and perpendicular deformation oscillations around the center of mass of the square patch. The amplitudes of these oscillations are decreasing with time. The system is in a steady state of rest for $t^+ \geq 1000$. The kinetic energy has decereased over approximately three orders of magnitude. The relative pressure in both phases is initialized with $p_{rel} = 0$. It is subsequently explicitly calculated from the pressure-density relation given by the Tait equation (Eq. 13). In order to avoid smearing of the density discontinuity at the phase interface, Eq. 9 is applied to calculate the rate of change of density. To prevent large scale oscillations and instabilities of the system, the dynamic viscosity in both phases is set to $\mu = 1 \cdot 10^{-2} Pa\ s$. For a quantitative evaluation of the test case the average relative pressure in both phases is plotted over time in Fig. 5. Starting from an initially

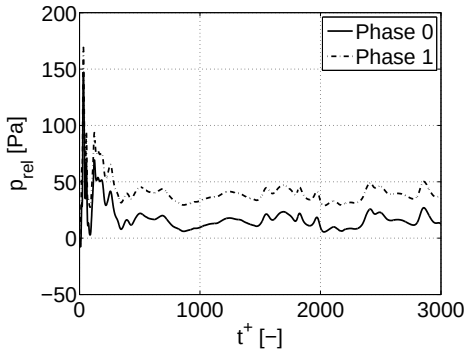

Figure 5. Oscillation of average pressure in both phases

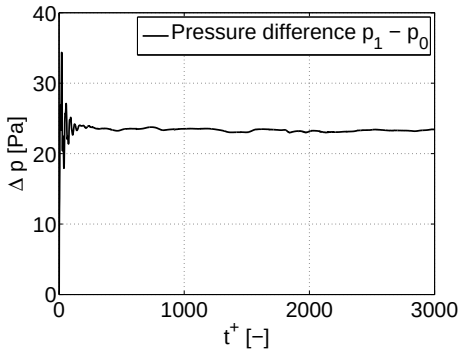

Figure 6. Pressure difference

non-equilibrated state, huge accelerations occur due to surface tension forces in regions of high curvature and the

system undergoes large pressure oscillations in its temporal evolution. The pressure difference, as depicted in Fig. 6, exhibits only minor fluctuations after $t^+ \simeq 1000$. From the Young-Laplace equation $\Delta p = \frac{\sigma}{R}$ a theoretical pressure difference of $\Delta p = \frac{\sigma}{R} = \frac{\sigma\sqrt{\pi}}{L_1} = 24.8\ Pa$ is derived under the assumption of incompressibility of both phases. The SPH simulation yields a pressure difference of $\Delta p = 23.4\ Pa$ in steady state. The relative error below 6% indicates a very good agreement between theory and numerical predicition taking into account the weakly compressible formulation of the SPH method.

Film disintegration

As technically relevant test case, the film disintegration at an airblast atomizer edge has been investigated. Corresponding experimental studies have been conducted by Gepperth et al. [17]. The experimental setup of the planar atomizer edge is depicted in Fig. 7. It was further simplified for the SPH predictions to be presented. The two-dimensional channel of height H and length L is confined by two inlets and the atomizer edge on the left, an outlet on the right and moving walls on top and bottom. The film of fluid 1 enters the computational domain via the inlet above the atomizer edge. At the inlets identical piecewise linear velocity profiles are imposed. The moving wall velocity is identical to the maximum inlet velocity $u_{max} = 1\ m/s$, representing the free-stream velocity of the surrounding fluid 0. For the three dimensional case front and back sections are modelled by periodic boundary conditions.

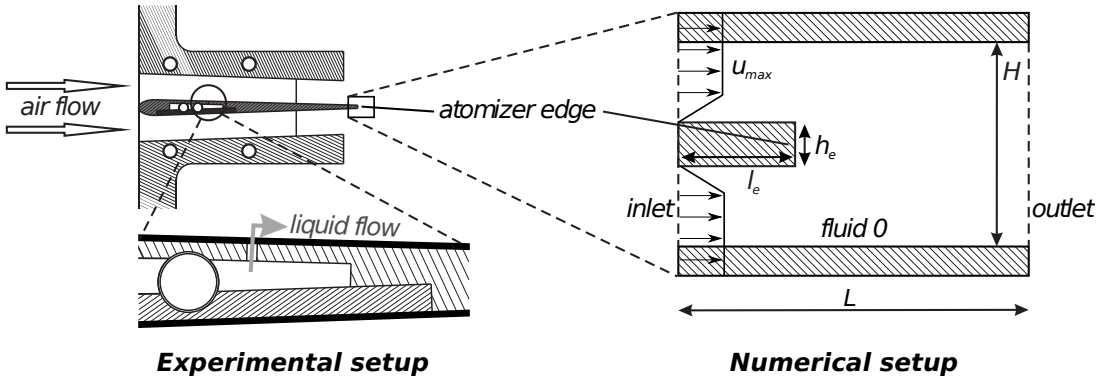

Figure 7. Experimental and numerical setup for film disintegration investigations

The walls consist of two staggered rows of fixed particles, the fluid domain is initially discretized by 5290 fluid particles. The viscosity ratio of both fluids is set to $\mu_1/\mu_0 = 5$, whereas density is identical. Surface tension is taken into account via the CSF model using $\sigma = 0.07\ N/m$.

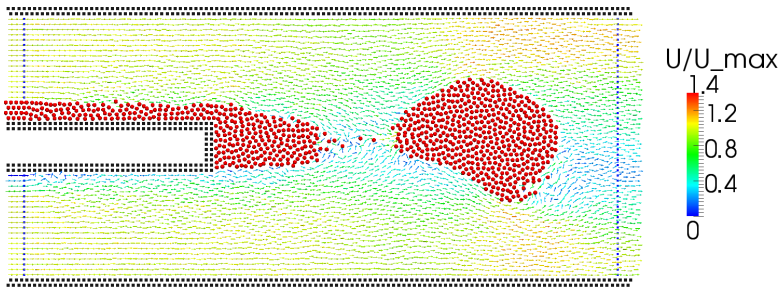

Figure 8. Film disintegration and shear-off of a liquid ligament

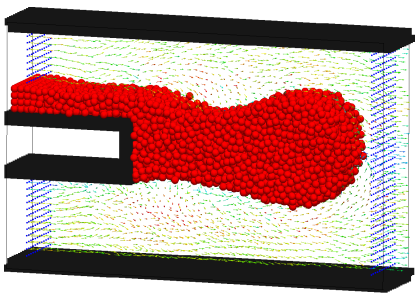

Figure 9. Three-dimensional film disintegration at atomizer edge

The results are displayed in Fig. 8 and 9. The typical characteristics of primary atomization are clearly visible in two- and three-dimensional simulations. The particles representing fluid 0 are depicted as colored arrows corresponding to the velocity field. Fluid 1 is depicted as red spheres. It is accumulated at the trailing edge of the atomizer lip due to surface tension forces and finally sheared off. After the ligament is detached from the atomizer edge, a droplet is formed.

Summary and Conclusions

A fully three-dimensional meshfree, Lagrangian particle code, based on the Smoothed Particle Hydrodynamics method has been developed. Test cases conducted so far prove the capability of this meshless method to correctly predict single as well as multiphase flows. The code has been successfully validated by the simulation of a Couette flow at different Reynolds numbers and the modeling of the pressure jump across a curved surface. Thus, the physical effects crucial for primary atomization can be captured. The additional implementation of versatile inlet and outlet boundaries offers the potential to efficiently simulate flow phenomena occuring in technically relevant systems. This was demonstrated by the simulation of film disintegration, which is a typical feature in airblast atomizers. The next step will be the tuning of the fluid properties and velocities for the three-dimensional atomizer edge test case to meet realistic engine conditions.

Acknowledgements

The current work has been partly financially supported by the European Commission under contract FP7-AAT-2010-RTD-1 within the 7th framework project "Fuel Injector Research for Sustainable Transport" (FIRST). The financial support is gratefully acknowledged.

Nomenclature

c	sound speed [m·s^{-1}]	H	channel height [m]
f	arbitrary spatial function [-]	L	scaling length [m]
h	smoothing length [m]	M	Mach number [-]
k	thermal conductivity [W·m^{-1}·K^{-1}]	R	radius [m]
m	mass [kg]	T	temperature [K]
n	normal vector [m]	W	kernel function [m^{-3}]
p	pressure [Pa]	γ	isentropic exponent [-]
r	position [m]	ζ	color index [-]
t	time [s]	μ	dynamic viscosity [Pa·s]
u	internal energy [J·kg^{-1}]	ρ	density [kg·m^{-3}]
v	velocity [m·s^{-1}]	σ	surface tension coefficient [N m^{-1}]
z	coordinate direction [m]	τ	shear stress [Pa]
		Φ	dissipation term [J·kg^{-1}·s^{-1}]

References

[1] Gingold, R. A., Monaghan, J. J, *Monthly Notices of the Royal Astronomical Society* 181: 375-389 (1977)
[2] Lucy. L. B., *The Astronomical Journal* 82: 1013-1024 (1977)
[3] Ménard, T., Tanguy, S., and Berlemont, A., *International Journal of Multiphase Flow* 33: 510-524 (2007)
[4] Fuster, D., et al., *International Journal of Multiphase Flow* 35; 550-565 (2009)
[5] Hoefler, C., Braun, S., Koch, R., and Bauer, H.-J., *Proc. 24th European Conference on Liquid Atomization and Spray Systems, Estoril, Portugal*, 2011
[6] Liu, M., Liu, G., *Archives of Computational Methods in Engineering* 17: 25-76 (2010)
[7] Monaghan, J. J., *Annual Review of Astronomy and Astrophysics* 30: 543-574 (1992)
[8] Colagrossi, A., Landrini, M., *Journal of Computational Physics* 191: 448-475 (2003)
[9] Morris, J., *PhD thesis: Analysis of Smoothed Particle Hydrodynamics with Applications*, Monash University (1996)
[10] Morris, J., Fox, P., and Zhu, Y., *Journal of Computational Physics* 136: 214-226 (1997)
[11] Cole, R., *Underwater Explosions* Princeton University Press, 1984
[12] Brackbill, J., Kothe, D., and Zemach, C., *Journal of Computational Physics* 100: 335-354 (1992)
[13] Morris, J., *International Journal for Numerical Methods in Fluids* 33: 333-353 (2000)
[14] Lastiwka, M., Basa, M., and Quinlan, N. J., *International Journal for Numerical Methods in Fluids* 61: 709-724 (2009)
[15] S. Majid Hosseini , James J. Feng, *Journal of Computational Physics* 230-19: 7473-7487 (2011)
[16] Shepard, D. *ACM National Conference* 23: 517-524 (1968)
[17] Gepperth, S., Guildenbecher, D., Koch, R. and Bauer, H.-J., *Proc. 23rd Annual Conference on Liquid Atomization and Spray Systems, Brno, Czech Republic*, 2010